International Journal of Nanomedicine

Dovepress
open access to scientific and medical research

Open Access Full Text Article

ORIGINAL RESEARCH

Synthesis and characterization of silver/montmorillonite/chitosan bionanocomposites by chemical reduction method and their antibacterial activity

This article was published in the following Dove Press journal:
International Journal of Nanomedicine
26 January 2011
Number of times this article has been viewed

Kamyar Shameli[1]
Mansor Bin Ahmad[1]
Mohsen Zargar[3]
Wan Md Zin Wan Yunus[1]
Nor Azowa Ibrahim[1]
Parvaneh Shabanzadeh[2]
Mansour Ghaffari Moghaddam[4]

[1]Department of Chemistry, Faculty of Science, [2]Institute for Mathematical Research, Universiti Putra Malaysia, Selangor, Malaysia; [3]Department of Biology, Islamic Azad University, Qum, Iran; [4]Department of Chemistry, Faculty of Science, University of Zabol, Zabol, Iran

Abstract: Silver nanoparticles (AgNPs) of a small size were successfully synthesized using the wet chemical reduction method into the lamellar space layer of montmorillonite/chitosan (MMT/Cts) as an organomodified mineral solid support in the absence of any heat treatment. $AgNO_3$, MMT, Cts, and $NaBH_4$ were used as the silver precursor, the solid support, the natural polymeric stabilizer, and the chemical reduction agent, respectively. MMT was suspended in aqueous $AgNO_3$/Cts solution. The interlamellar space limits were changed (d-spacing = 1.24–1.54 nm); therefore, AgNPs formed on the interlayer and external surface of MMT/Cts with d-average = 6.28–9.84 nm diameter. Characterizations were done using different methods, ie, ultraviolet-visible spectroscopy, powder X-ray diffraction, transmission electron microscopy, scanning electron microscopy, energy dispersive X-ray fluorescence spectrometry, and Fourier transform infrared spectroscopy. Silver/montmorillonite/chitosan bionanocomposite (Ag/MMT/Cts BNC) systems were examined. The antibacterial activity of AgNPs in MMT/Cts was investigated against Gram-positive bacteria, ie, *Staphylococcus aureus* and methicillin-resistant *S. aureus* and Gram-negative bacteria, ie, *Escherichia coli*, *E. coli* O157:H7, and *Pseudomonas aeruginosa* by the disc diffusion method using Mueller Hinton agar at different sizes of AgNPs. All of the synthesized Ag/MMT/Cts BNCs were found to have high antibacterial activity. These results show that Ag/MMT/Cts BNCs can be useful in different biological research and biomedical applications, including surgical devices and drug delivery vehicles.

Keywords: silver nanoparticles, bionanocomposites, montmorillonite, chitosan, antibacterial activity, Mueller Hinton agar

Introduction

In recent years, silver nanoparticles (AgNPs) have attracted considerable attention for medical and chemical applications due to their exceptional properties, including antibacterial activity, high resistance to oxidation, and high thermal conductivity.[1–5] Recently, different inorganic antibacterial materials, including AgNPs, have been expanded and some are in commercial use.[6] The antibacterial activity of AgNPs-containing materials can be used, for example, in medicines to treat infections in human skin,[7,8] dental materials,[9] catheters,[10,11] vascular grafts,[12] stainless steel materials,[13] arthroplasty,[14] and burn treatment,[15,16] as well as to prevent microorganism colonization on prostheses.[17] In addition, nanomaterials including AgNPs can be utilized for water treatment[18] and also for reducing bacteria on textile fabrics.[19,20] AgNPs also have effective cytoprotective activity towards human immunodeficiency virus-infected cells.[21] Because of this broad variety of applications, many preparation methods have

Correspondence: Kamyar Shameli
Department of Chemistry, Faculty of Science, Universiti Putra Malaysia, 43400, Serdang, Selangor, Malaysia
Tel +603 8946 6044
Fax +603 8946 6043
Email kamyarshameli@gmail.com

been developed. In addition to the bactericidal effects of Ag^+ ions, the antimicrobial activity of colloid AgNPs is influenced by the size of the particles, ie, the smaller the particles, the greater the antimicrobial effect.[22–28] Therefore, in developing methods for AgNP preparation, it is important to control the size of the AgNP particles. AgNPs of small size and devoid of aggregation properties are favorable for this purpose.

Chemical reduction methods have been widely investigated for the synthesis of AgNPs because these techniques can be executed under easy and gentle conditions, and can be used to synthesize AgNPs on a large scale. The reducing capability of a reductant has a significant role in the synthesis of AgNPs by the reduction reaction. The use of a strong reducing agent, such as $NaBH_4$, results in tiny particles that are well dispersed.[29]

Nowadays, a succession of chemical reductants can been used for the synthesis of noble metal nanoparticles which contain $NaBH_4$,[30,31,36] NH_2OH,[32] N_2H_4,[33,36] $(CH_3)_2NH{\cdot}BH_3$,[34] H_2,[35] formaldehyde,[36] formamide,[37] Tollens' reagents,[38] ethylene glycol,[39] ethanol,[40] citrate,[32,40] aniline,[41] polyaniline,[42] or ascorbic acid.[43]

Layered silicates, eg, montmorillonite (MMT), have been used in polymer nanocomposites with a significant improvement in mechanical properties.[44,45] MMT possesses a 2-to-1 layered structure with a single octahedral aluminum layer located between two layers of tetrahedral silicon.[46] Each layer is about 1 nm thick with a lateral dimension of 100–1000 nm.[47] Furthermore, being a lamellar clay, MMT has intercalation, swelling, and ion exchange properties.[48] MMT can be delaminated into elemental sheets without difficulty. Therefore, it is tempting to utilize these sheets as the substrate for preparation of nanoscale metals by means of electrodeless plating. The MMT interlayer space has been used for the synthesis of material and biomaterial nanoparticles as the support for anchoring transition metal complexes and as adsorbents for cationic ions.[49,50]

Among the natural polymers, chitosan (Cts) has been extensively investigated as a natural cationic biopolymer because of its excellent biocompatibility, biodegradability, nontoxicity, bioactivity, and multifunctional groups, as well as its solubility in aqueous medium for food packaging film, bone substitutes, and artificial skin.[51] Cts can be intercalated in MMT by cationic exchange and hydrogen bonding processes, whereby the resulting bionanocomposites (BNCs) show interesting structural and functional properties.[52] Conversely, BNCs are made of a natural polymeric matrix and inorganic/organic filler with at least one dimension on the nanometer scale. Metal/clay/polymer compounds like BNCs with their excellent properties have become a promising new areas of research.[53]

Furthermore, AgNPs have long been known to have strong inhibitory and bactericidal effects, as well as a broad spectrum of antimicrobial activity, and have been used for centuries to prevent and treat a variety of diseases, most notably infections. AgNPs were reported recently as having antibacterial activity against *Escherichia coli*, *Staphylococcus aureus*, methicillin-resistant *Staphylococcus epidermis*, and methicillin-resistant *S. aureus* (MRSA) bacteria.[53–55] AgNPs also exhibit potent cytoprotective activity towards cells infected with human immunodeficiency virus.[56] The application of AgNPs for biological labelling in neuroblastoma cells was recently reported. Due to the strong plasmon-resonant properties of AgNPs and the enhanced resolution obtainable with high-illumination systems in physiological solution, studies of the interactions between AgNPs and human cells have been possible.[57] Hence, similar studies on Ag/poly(lactic acid),[30] Ag/MMT,[48,59] Ag/talc,[58] Ag/MMT/starch BNCs[60] and Ag/MMT/Cts BNCs,[61,62] have been undertaken previously.

In this research, the spherical structure of AgNPs was synthesized in the interlayer surface of the MMT layers modified with a low percentage of Cts in aqueous solution by using $AgNO_3$, Cts, and $NaBH_4$ as the silver precursor, the stabilizer, and the reduction agent, respectively, at room temperature. We used modified clay (MMT/Cts) as the protective colloid to prevent the AgNPs from aggregating, and it was found that MMT/Cts also assisted in the chemical reduction process of silver. Needless to say, to date, there has not been any report of a study of Ag/MMT/Cts BNCs using a chemical reduction method, ie, lamellar polymeric silicate, which is the subject of this research. In addition, the antibacterial activity of $AgNO_3$/MMT/Cts and Ag/MMT/Cts BNCs were investigated and compared. Using this method, we were able to obtain AgNPs of different sizes and dissimilar antibacterial activity by controlling the $AgNO_3$ concentration.

Materials and methods

Chemicals

All reagents in this work were of analytical grade and used as received without further purification. $AgNO_3$ (99.98%), used as the silver precursor, was obtained from Merck (Darmstadt, Germany). Meanwhile, the MMT powder, used as a solid support for the AgNPs, was purchased from Kunipia-F (Tokyo, Japan). $NaBH_4$ (98.5%), low-molecular-weight Cts, and glacial acetic acid (99%) used as a reduction agent, a stabilizer, and for solubilizing Cts, respectively, were obtained from

Sigma-Aldrich (St Louis, MO). All the aqueous solutions were used with double-distilled water.

Synthesis of Ag/MMT/Cts BNCs using $NaBH_4$

For the synthesis of Ag/MMT/Cts BNCs, soluble Cts (100 mL, 0.5 wt%) was prepared by solubilization in 1.0 wt% of acetic acid solution (pH ~3.53) under constant stirring for 45 minutes, for each of the samples. Following the usual preparation method for AgNPs, $AgNO_3$ solutions were added to each soluble Cts sample under constant stirring for synthesis of the $AgNO_3$/Cts solutions. The aqueous Cts-acetic acid solution thickened after the addition of $AgNO_3$ solution. The Ag content of the samples was 0.5 (A1), 1.0 (A2), 1.5 (A3), 2.0 (A4), and 5.0 g (A5) Ag/100 g MMT. Constant amounts of MMT were suspended in different volumes of 1×10^{-3} M $AgNO_3$ solution with soluble Cts and stirred for 24 hours at room temperature to obtain the $AgNO_3$/MMT/Cts suspensions. Freshly prepared $NaBH_4$ (4×10^{-2} M) solution was then added to the suspensions under continuous stirring to reach a constant $AgNO_3/NaBH_4$ molar ratio (1:4). After the addition of the reducing agent, stirring was continued for another hour. The suspensions of Ag/MMT/Cts BNCs obtained were then centrifuged, washed four times using double-distilled water to remove the silver ion residue, and dried at 40°C under vacuum overnight. All the experiments were conducted at ambient temperature.

Evaluation of antibacterial activity

The in vitro antibacterial activity of the samples was evaluated by the disc diffusion method using Mueller Hinton agar with determination of inhibition zones, which conformed to the recommended standards of the National Committee for Clinical Laboratory Standards (now known as the Clinical and Laboratory Standards Institute, 2000). *E. coli* (ATCC 25922), *E. coli* O157:H7 (ATCC 43895), *Pseudomonas aeruginosa* (ATCC 10145), *S. aureus* (ATCC 25923), and MRSA (ATCC 700689) were used for the antibacterial assay. Briefly, 6 mm sterile paper discs impregnated with 20 µL of Ag/MMT/Cts BNCs (A2, A4, and A5) with different treatment times were suspended in the sterile distilled water and left to dry at 37°C for 24 hours under sterile conditions. The bacterial suspension was prepared by making a saline suspension of isolated colonies selected over 18–24 hours of tryptic soy agar plate. The suspension was adjusted to match the tube of 0.5 McFarland turbidity standard using the spectrophotometer at 600 nm, which is equivalent to 1.5×10^8 colony-forming units/mL. The surface of the Mueller Hinton agar was completely inoculated using a sterile swab, and was then steeped in the prepared suspension of bacterium. Finally, the impregnated discs were placed on the inoculated agar and incubated at 37°C for 24 hours. After incubation, the diameter of the growth inhibition zones was measured. Chloramphenicol 30 µg and cefotaxime 30 µg were used as the positive standards in order to control the sensitivity of the bacteria. All tests were done in triplicate.

Characterization methods and instruments

The prepared Ag/MMT/Cts BNCs were characterized by ultraviolet (UV)-visible spectroscopy, powder X-ray diffraction (PXRD), transmission electron microscopy (TEM), scanning electron microscopy (SEM), energy dispersive X-ray fluorescence spectrometry (EDXRF), inductively coupled plasma-optical emission spectrophotometer (ICP-OES), and Fourier transform infrared (FT-IR) spectroscopy. The UV-visible spectra were recorded over the 300–700 nm range utilising the Shimadzu H.UV.1650 PC spectrophotometer. The structures of the Ag/MMT/Cts BNCs produced were examined by powder X-ray diffraction using the Shimadzu PXRD-6000. Changes in the interlamellar spacing of MMT and Ag/MMT/Cts BNCs were also studied by PXRD in the angle range of $2° < 2\theta < 12°$. In addition, the interlamellar spaces were calculated from the PXRD peak positions using Bragg's law. A wavelength (λ) of 0.15418 nm was used for these measurements. The PXRD patterns were recorded at a scan speed of 2° min^{-1}. TEM observations were carried out on a H-7100 electron microscope (Hitachi, Tokyo, Japan), and the particle size distributions were determined using the UTHSCSA Image Tool program (version 3.00; Dental Diagnostic Science, UTHSCSA, San Antonio, TX). SEM was performed using the Philips XL-30 instrument (Philips, Eindhoven, The Netherlands) to study the morphology of MMT, MMT/Cts, and Ag/MMT/Cts BNCs (A2, A4, and A5). EDXRF was carried out on a EDX-700HS spectrometer (Shimadzu, Osaka, Japan). Elemental analysis of the synthesized AgNPs was quantified using an ICP-OES, model Optima 2000DV (Perkin Elmer, Waltham, MA). Meanwhile, the FT-IR spectra were recorded over the range of 400–4000 cm^{-1} using the Series 100 Perkin Elmer FT-IR 1650 spectrophotometer. After the reactions, the samples were centrifuged using a high-speed centrifuge machine (Avanti J25; Beckman, Brea, CA).

Results and discussion

To prepare the stable AgNPs via the wet chemical reduction method, it was important to choose a suitable stabilizer and reducing agent. In this research, a MMT/Cts suspension was used as the appropriate support for reducing $AgNO_3$/MMT/Cts suspension, and using $NaBH_4$ as the strong reducing agent. $AgNO_3$ was reduced by $NaBH_4$ in the presence of MMT hydride with Cts (MMT/Cts), resulting in AgNPs prepared according to the following equation:[63]

$$Ag^{+}/MMT/Cts + BH_4^{-} + 3H_2O \rightarrow Ag^{0}/MMT/Cts + B(OH)_3 + 3.5H_2 \uparrow$$

The schematic illustration of the synthesis of Ag/MMT/Cts BNCs from $AgNO_3$/MMT/Cts produced using $NaBH_4$ as the chemical reduction agent is shown in Figure 1. Meanwhile, as shown in Figure 2, the MMT and $AgNO_3$/MMT/Cts suspensions (A0) were colorless, but after the addition of the reducing agent to the suspensions, they turned light brown (A1), brown (A2), reddish-brown (A3), and dark brown (A4 and A5), indicating the formation of AgNPs in the MMT/Cts suspensions. The formation of AgNPs was also followed by measuring the surface plasmon resonance bands of the $AgNO_3$/MMT/Cts (A0) and Ag/MMT/Cts BNCs suspensions (A1–A5) at wavelengths in the 300–700 nm range (Figure 3). The comparison between the PXRD patterns of MMT, MMT/Cts, and Ag/MMT/Cts BNCs (A1, A2, and A5) in the small angle range of 2θ ($2° < 2\theta < 12°$) indicated the formation of the intercalated AgNPs structure (Figure 4). In addition, the PXRD patterns in the wide angle range of 2θ ($30° < 2\theta < 80°$) were also employed to determine the crystalline structures of the synthesized AgNPs (Figure 5). The TEM images and size distribution of the AgNPs showed that the mean diameter of the nanoparticles ranged from about 6.28 nm to 9.84 nm (Figure 6). As shown in Figures 7 and 8, the SEM images indicated that there were no structural changes between the initial MMT, MMT/Cts, and Ag/MMT/Cts BNCs (A2, A4, and A5) at different $AgNO_3$ concentrations. In addition, the EDXRF spectra for the MMT, MMT/Cts and Ag/MMT/Cts BNCs (A2, A4, and A5) confirmed the presence of elemental compounds in MMT, Cts, and AgNPs without any other impurity peaks (Figures 7 and 8). The chemical structures of MMT, MMT/Cts, and Ag/MMT/Cts BNCs (A2, A4, and A5) were analyzed by FT-IR spectroscopy (Figures 9 and 10). The approximate efficiency gradually increased from A1 to A5, respectively (Table 1). The antibacterial studies showed comparatively similar effects for all samples, as indicated by the inhibition zone test between Cts, MMT/Cts, MMT, $AgNO_3$/MMT/Cts (A0),

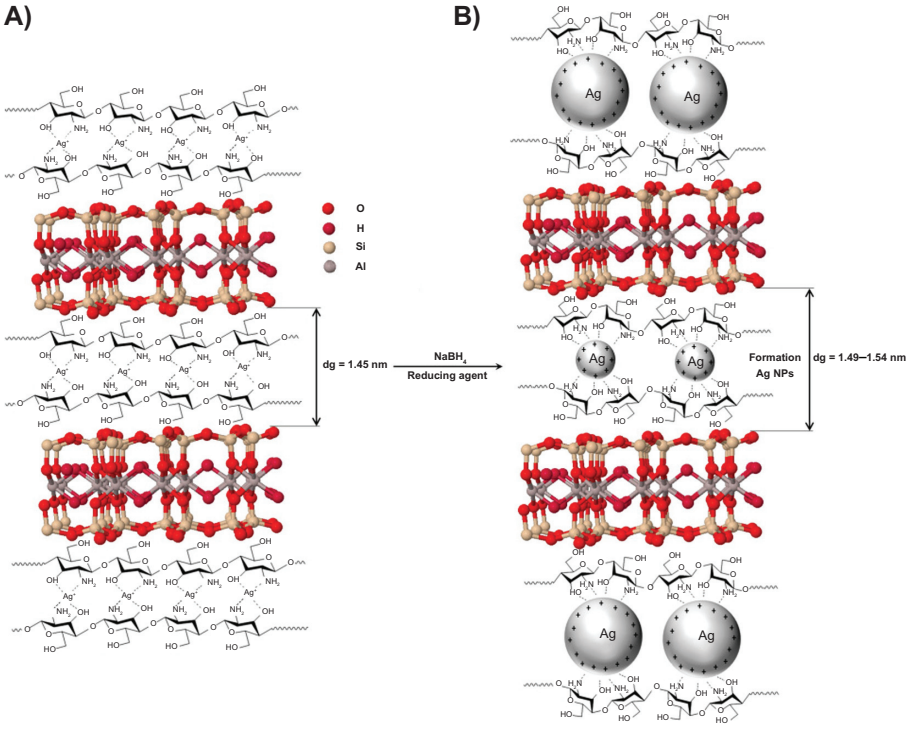

Figure 1 Schematic illustration of the synthesized silver/montmorillonite/chitosan bionanocomposites from silver nitrate/montmorillonite/chitosan (A0) by a chemical reduction method.
Abbreviations: AgNPs, silver nanoparticles.

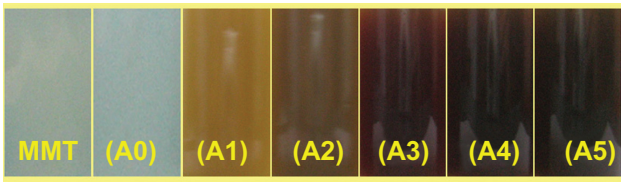

Figure 2 Photograph of montmorillonite/chitosan bionanocomposite suspension (A0) and silver/montmorillonite/chitosan bionanocomposite suspension at different $AgNO_3$ concentrations; (A1) 0.5%, (A2) 1.0%, (A3) 1.5%, (A4) 2.0%, and (A5) 5.0%.

and Ag/MMT/Cts BNCs (A2, A4, and A5) against different bacteria (Figure 11, Table 2).

Ultraviolet-visible spectroscopy

The color of the $AgNO_3$/MMT/Cts suspensions through the reduction process using $NaBH_4$ changed from colorless to light brown, brown, reddish-brown, and, finally, dark brown (A1–A5), respectively, which indicated the formation of AgNPs in the MMT/Cts suspension. The silver surface plasmon resonance bands were detected around 391–408 nm (Figure 3). These absorption bands were assumed to correspond to AgNPs smaller than 10 nm.[64] While there was no UV-visible absorption of AgNPs before the addition of $NaBH_4$ in A0 (Figure 3), the growth of the plasmon peak at 391 nm indicated the formation of AgNPs in A1. Furthermore, the gradual increase in the $AgNO_3$ concentration from A1 to A4 also increased the corresponding peak intensities in the wavelength range of 391–403 nm. In A5, the absorption peak due to surface plasmon resonance of Ag^+ was slightly red-shifted to a higher wavelength (408 nm), which indicated the increase in size of the AgNPs.[65,66]

Powder X-ray diffraction

As shown in Figure 4, the original d-spacing (d_S) of MMT (1.24 nm) and in MMT/Cts, was increased to 1.45 nm at the small 2θ angles (2θ = 7.12° for MMT and 2θ = 6.09° for MMT/Cts) by Cts intercalation. The d_S in A2, A4, and

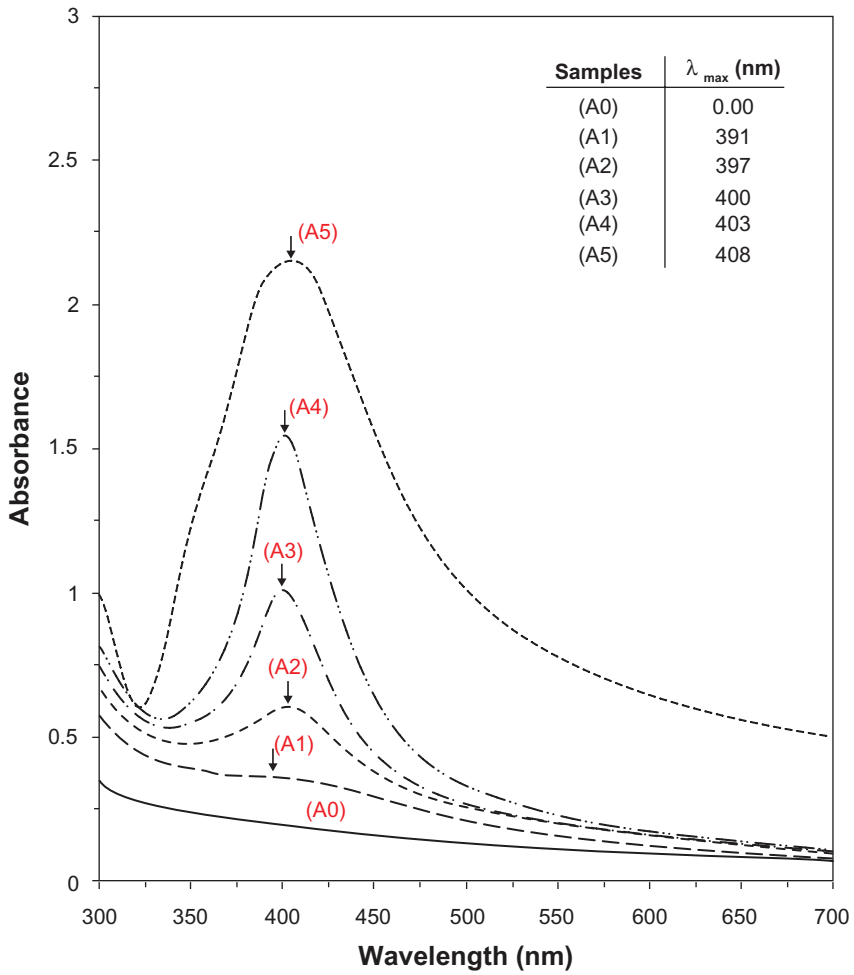

Figure 3 Ultraviolet-visible absorption spectra of silver/montmorillonite/chitosan bionanocomposite suspension for different $AgNO_3$ concentrations: (A1) 0.5%, (A2) 1.0%, (A3) 1.5%, (A4) 2.0%, (A5) 5.0%, and (A0) silver nitrate/montmorillonite/chitosan bionanocomposite suspension in the absence of sodium borohydride.

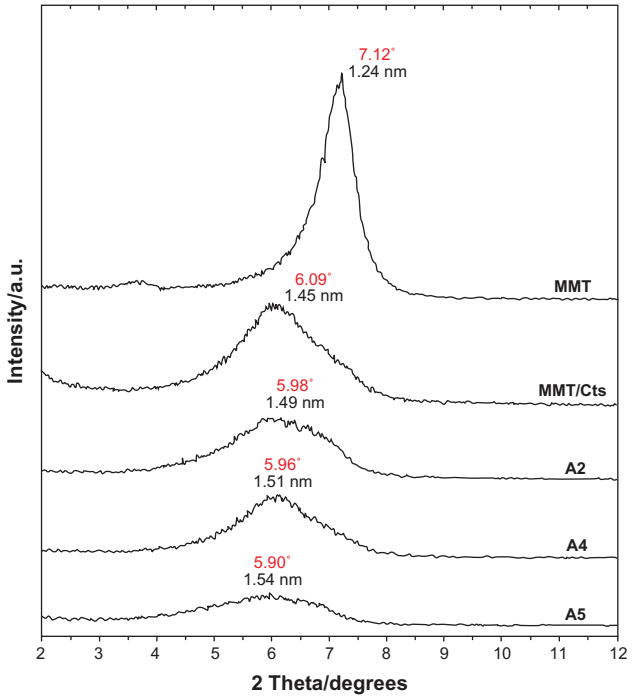

Figure 4 Powder X-ray diffraction patterns of montmorillonite, montmorillonite/chitosan, and silver/montmorillonite/chitosan bionanocomposites for determination of d-spacing at different $AgNO_3$ concentrations: (A2) 1.0%, (A4) 2.0%, and (A5) 5.0%.

Abbreviations: Cts, chitosan; MMT, montmorillonite.

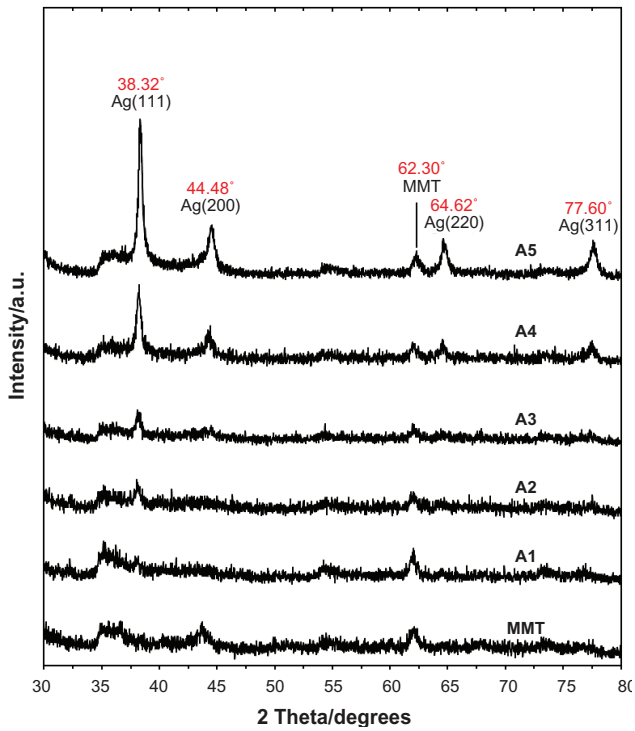

Figure 5 Powder X-ray diffraction patterns of montmorillonite and silver/montmorillonite/chitosan bionanocomposites for determination of silver crystals at different $AgNO_3$ concentrations: (A1) 0.5%, (A2) 1.0%, (A3) 1.5%, (A4) 2.0%, and (A5) 5.0%.

Abbreviation: MMT, montmorillonite.

A5 also increased gradually from 1.49 nm to 1.51 nm and finally to 1.54 nm at the 2θ angles (2θ = 5.98° [A1], 2θ = 5.96° [A4], and 2θ = 5.90° [A5]) by Ag/Cts intercalation between MMT layers. These d_S values were direct proof of the intercalation structures. The AgNPs formed at the latter location were the cause of the increase in basal spacing. In these samples, the intensities of the reflections were significantly lower, whereas their half-widths were larger than those of undoped clay minerals, whereby the highly ordered parallel lamellar structure of the mineral was disrupted by metal nanoparticle formation.[67] In addition, all the Ag/MMT/Cts BNCs (A1–A5) had a similar diffraction profile, and the PXRD peaks at 2θ of 38.32°, 44.48°, 64.62°, and 77.60° (Figure 5) could be attributed to the 111, 200, 220, and 311 crystallographic planes of the face-centered cubic silver crystals, respectively.[68] For all samples, the main crystalline phase was silver, and no other obvious phases were found as impurities in the PXRD patterns. Moreover, the PXRD peak broadenings of the AgNPs were mostly due to the existing nanosized particles in the BNPs. In addition, there was a characteristic peak at about 2θ = 62.30° related to the MMT clay (PXRD Ref No 00–003–0010) as a stable substrate. The intensities of 111, 200, 220, and 311 reflections due to the AgNP phase were also found to increase along with the increased AgNPs in the solid support matrix content stabilizer (MMT/Cts) by the wet chemical reduction method.

Morphology

The TEM images and their corresponding particle size distributions for the Ag/MMT/Cts BNCs containing different percentages of AgNPs are shown in Figure 6. The TEM images and their size distributions reveal that the mean diameters and standard deviation of the AgNPs were about 6.28 ± 3.54, 8.29 ± 3.18, and 9.84 ± 2.51 nm for 1.0% (A-B), 2.0% (C-D) and 5.0% (E-F), respectively. These results showed that the diameters of the AgNPs synthesized by this method depended on the initial $AgNO_3$ concentration. SEM images of the MMT, MMT/Cts, and Ag/MMT/Cts (A2, A4, and A5) are presented in Figures 7 and 8. The surface morphology of MMT demonstrates a layered surface with some large flakes, which is the typical structure for MMT (Figure 7A). The exterior morphology of the MMT/Cts and Ag/MMT/Cts BNCs (A2, A4, and A5), show layered surfaces with large flakes and without significant morphological differences between them. Furthermore, the external surfaces of Ag/MMT/Cts BNCs (A2, A4, and A5) gradually become more shiny due to the presence and increase of AgNP amounts

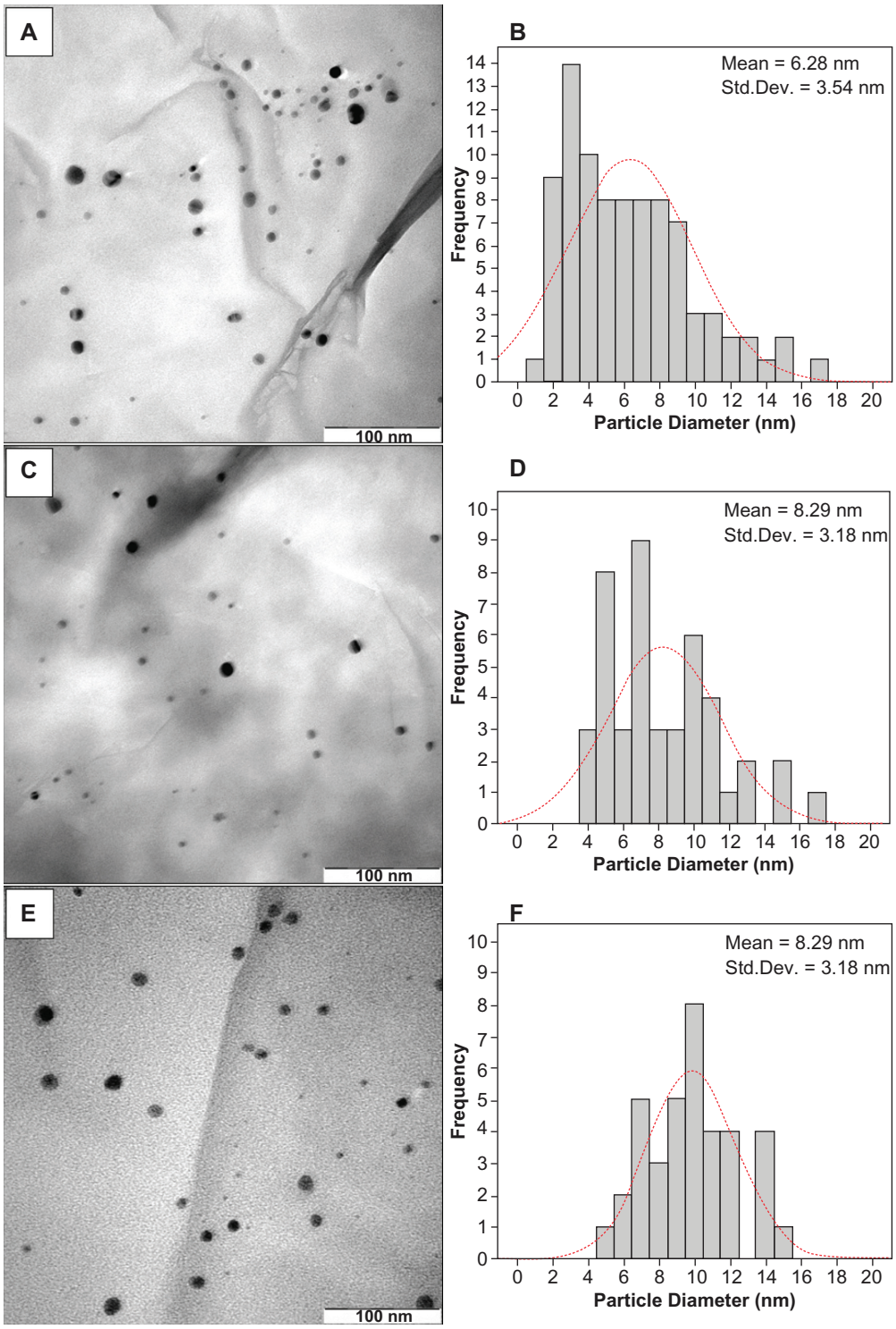

Figure 6 Transmission electron microscopy images and corresponding particle size distribution of silver/montmorillonite/chitosan bionanocomposites at different $AgNO_3$ concentrations: 1.0% (**A**, **B**), 2.0% (**C**, **D**), and 5.0% (**E**, **F**).

(Figures 8 A, B, and C). Figure 7 (B, D) shows the EDXRF spectra for the MMT and MMT/Cts. The peaks at around 1.7, 2.7, 2.9, 3.7, 4.0, 4.5, 6.4, and 7.1 keV are related to the binding energies of MMT, and peaks at around 8.1, 8.7, and 9.6 keV correspond to the binding energies of Cts. In Figure 8D, the peaks around 1.3, 3.1, 3.3, and 3.4 keV are related to Ag^+ elements in A2, A4, and A5.[69] In addition, the EDXRF spectra for the MMT, MMT/Cts, and Ag/MMT/Cts BNCs (A2, A4, and A5) confirmed the presence of elemental compounds in the MMT, Cts, and AgNPs without any impurity peaks.

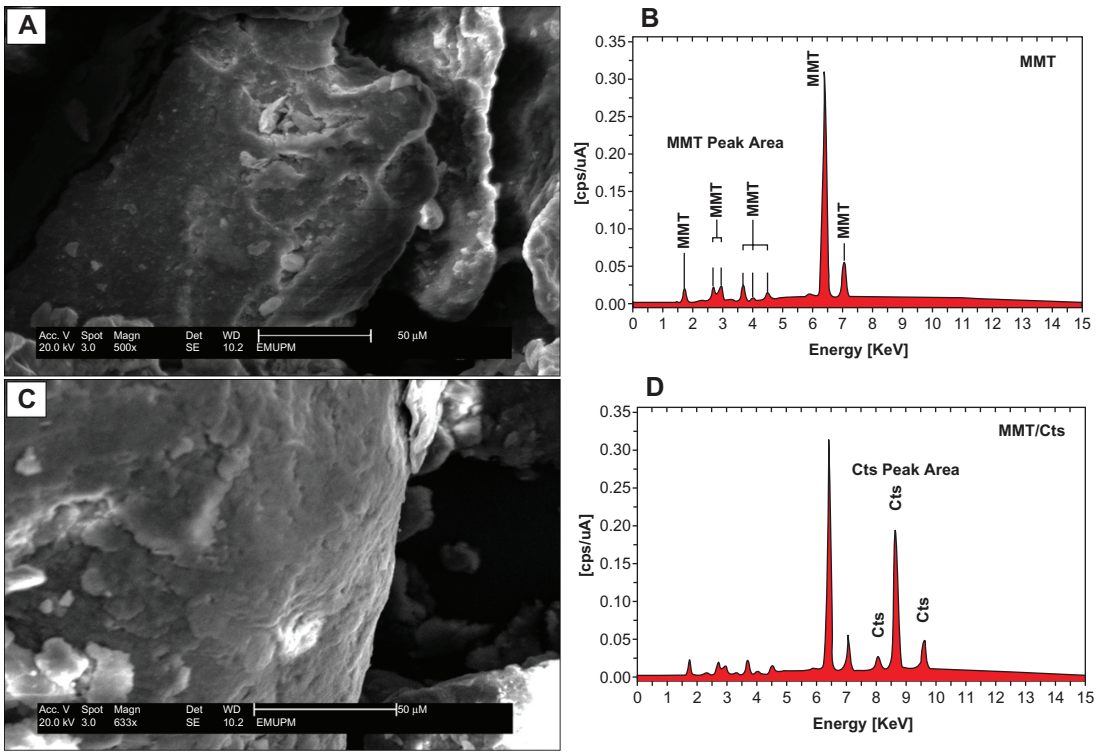

Figure 7 Scanning electron microscopy micrographs and energy dispersive X-ray fluorescence spectra for montmorillonite (**A**, **B**) and montmorillonite/chitosan (**C**, **D**), respectively.
Abbreviations: Cts, chitosan; MMT, montmorillonite.

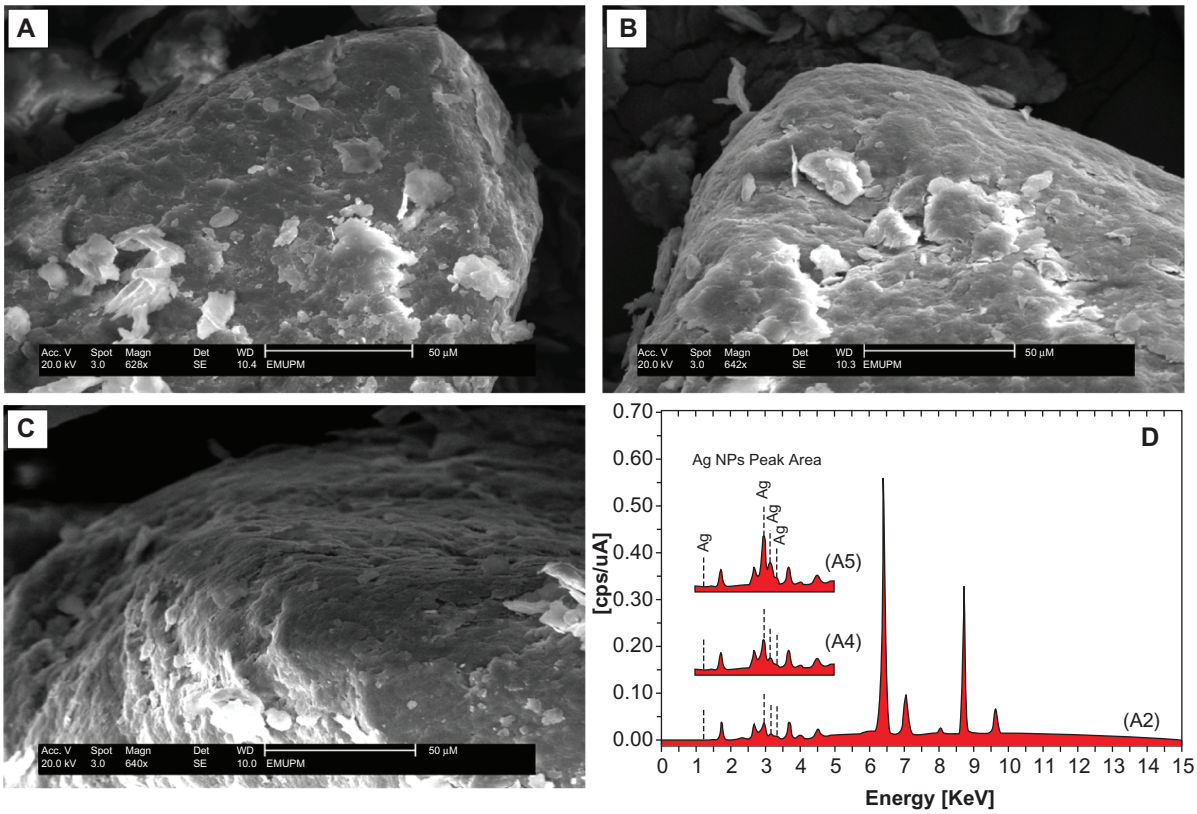

Figure 8 Scanning electron micrographs and energy dispersive X-ray fluorescence spectra, respectively, for the silver/montmorillonite/chitosan bionanocomposites at different $AgNO_3$ concentrations: 1.0% (**A**), 2.0% (**B**), 5.0% (**C**), and (**D**).
Abbreviation: AgNPs, silver nanoparticles.

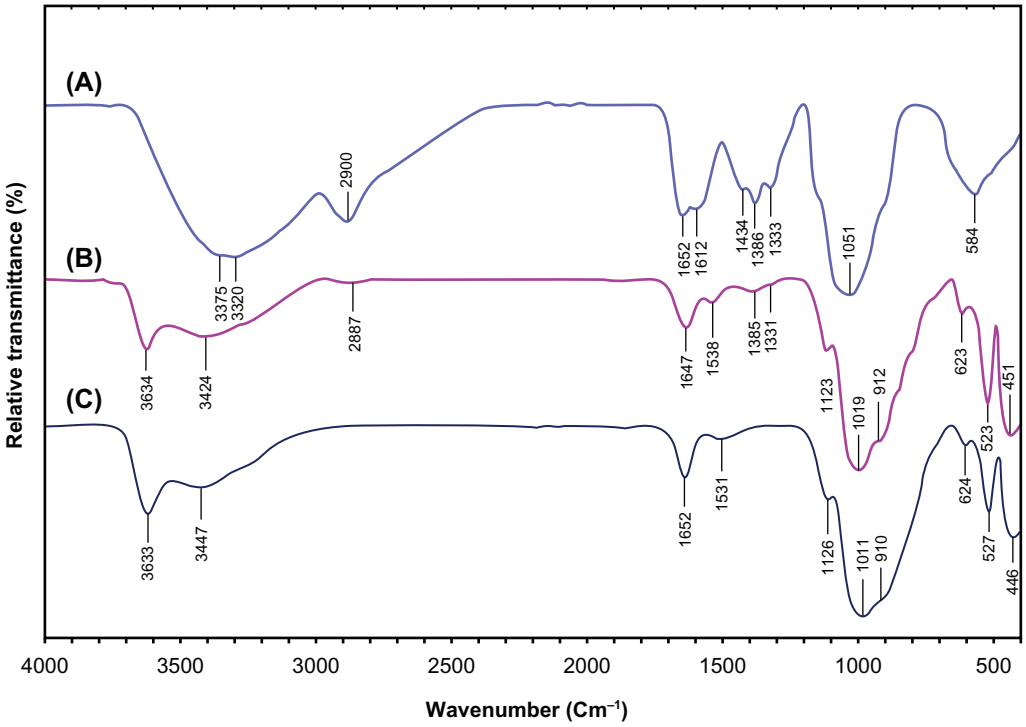

Figure 9 Fourier transform infrared spectra for chitosan (**A**), montmorillonite/chitosan (**B**), and montmorillonite (**C**), respectively.

Figure 8D also demonstrates that, with the increased percentages of AgNPs in MMT/Cts (1%, 2%, and 5%) and after reduction, the intensity of AgNP peaks in the EDXRF spectra increased. The results indicate that the synthesized BNCs are composed of high-purity Cts and AgNPs.

Chemical analysis by Fourier transform infrared spectroscopy

The FT-IR spectrum of MMT (Figure 9C) show the vibration bands at 3633 cm^{-1} for O-H stretching, 3447 cm^{-1} due to the interlayered O-H stretching (H bonding), at 1652 and 1531 cm^{-1} for H-O-H bending, 1126, 1011, and 910 cm^{-1} for Si-O stretching, 624 cm^{-1} for Al-OH, 910 cm^{-1} due to (Al, Mg)-OH vibration modes and 527 and 446 cm^{-1} for Si-O bending.[70] The spectrum of Cts (Figure 9A) show peaks at 3375 and 3320 cm^{-1} due to the overlapping of O-H and N-H stretching bands, ie, 2900 cm^{-1} for aliphatic C-H stretching, 1652 and 1612 cm^{-1} for N-H bending, 1434, 1386, and 1333 cm^{-1} for C-H bending, and 1051 cm^{-1} for C-O stretching. The spectrum of MMT/Cts (Figure 9B) shows a combination of characteristic absorptions due to MMT and the amine groups of Cts. The peaks of the external vibration and interlayered stretching O-H groups in MMT and MMT/Cts were relatively constant at 3634, and a little shifted to low wave numbers in 3424 cm^{-1}. On the other hand, the peaks of aliphatic C-H and -NH_2 groups in pure Cts at 2900, 1652, and 1612 cm^{-1} were shifted to 2887, 1647, and 1538 cm^{-1} in the MMT/Cts, corresponding to the deformation vibration of the amine group of Cts.[71,72] These results appeared to be in agreement with the data from PXRD, revealing the intercalation of Cts in the MMT structure.

As shown in Figure 10, there were changes in the spectra of Ag/MMT/Cts BNCs compared with MMT/Cts (Figure 9) and peaks in A2, A4, and A5 shifted to lower wave numbers. The FT-IR spectra demonstrated the inflexibility of the silicate layers and the nonbonding chemical interface between the silicate layers and AgNPs in Ag/MMT/Cts BNCs (A2, A4, and A5). The interactions between the silicate layers of MMT and Cts were related to the peaks at the high and low wave numbers. For example in A2, a peak at 2946 cm^{-1} is associated with aliphatic C-H stretching, at 1649 cm^{-1} is related to the overlap Cts peaks in 1652 and 1612 cm^{-1}, with a MMT peak in 1652 cm^{-1}. Moreover, peaks appear in 1448, 1396, and 1330 cm^{-1} connected with C-H bending, similar to the Cts peaks. Broad peaks were due to the presence of van der Waals interactions between the hydroxyl, amine, and C-H bending groups of Cts intercalated to the MMT layers with a partial positive charge on the surface of the AgNPs.[61] These results confirm that, with the increased amounts of AgNPs in the Ag/MMT/Cts BNCs (A2, A4, and A5), respectively, due to the existence of complexation peaks between the Cts groups and AgNPs, the peaks are shifted to low wave numbers and the peak intensity is increased.

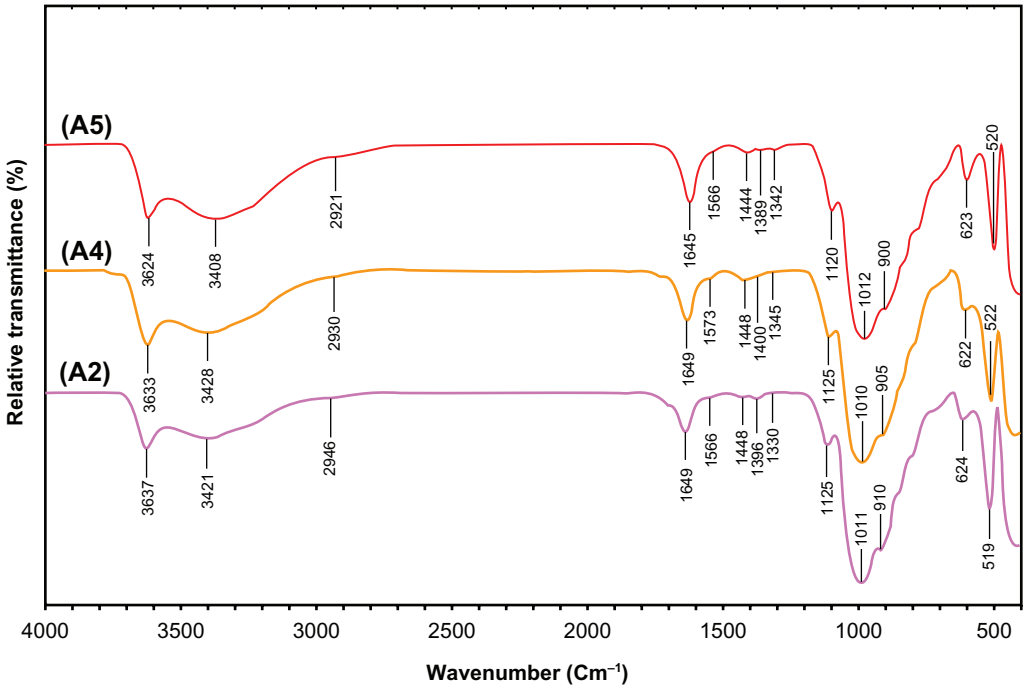

Figure 10 Fourier transform infrared spectra for the silver/montmorillonite/chitosan bionanocomposites at different $AgNO_3$ concentrations: (A2) 1.0% (**A**), (A4) 2.0% (**B**), and (A5) 5.0% (**C**).

Inductively coupled plasma-optical emission spectroscopy

The ICP-OES analyzer was used to determine the approximate efficiency of $AgNO_3$/MMT/Cts suspension reduction by $NaBH_4$ to Ag/MMT/Cts BNCs. A modified digestion method was used to quantify the amount of AgNP conversion to Ag^+ in the MMT/Cts. An air-dried mass of each Ag/MMT/Cts BNC sample (A1–A5) was submerged in a solution of 10 mL of ultrapure reagent grade nitric acid (364576, grade >90%; Sigma-Aldrich), and 10 mL of double-distilled water. After the samples were placed over the digestion beakers, the solutions were heated to approximately 80°C for 15 minutes and allowed to react. The digestion solutions were allowed to cool in room temperature and then filtered through a glass fiber filter (Qualitative #2; Whatman, Florham Park, NJ) and diluted in 100 mL in volumetric flasks.[73] After detecting the Ag^+ ions by ICP-OES spectroscopy, with the increased concentration of $AgNO_3$ in the MMT/Cts matrix and then the reduction by the reducing agent, the approximate efficiency gradually decreased from 97.20% to 95.35%, 92.47%, 88.53%, and, finally, 83.50% after A1, A2, A3, A4, and A5, respectively (Table 1). The results from the ICP-OES analysis using a strong reduction agent confirmed the formation of AgNPs in MMT/Cts, which produced high yields.

Antibacterial activity

Inhibition zone values were obtained for the synthesized $AgNO_3$/MMT/Cts suspension and Ag/MMT/Cts BNCs (A2, A4, and A5) tested against *E. coli*, *E. coli* O157:H7,

Table 1 Physical properties of silver nanoparticles in silver/montmorillonite/chitosan bionanocomposites synthesised at different $AgNO_3$ concentrations: (A1) 0.5%, (A2) 1.0%, (A3) 1.5%, (A4) 2.0%, and (A5) 5.0%

Samples	Reaction volume (Lit)	λ max[a]	Absorbance[b]	Approximated efficiency (%)	Ag nanoparticle size[c] (nm)
A1	0.50	391	0.44	97.20 ± 2.35	5.42 ± 2.15
A2	1.00	397	0.69	95.35 ± 2.88	6.28 ± 3.54
A3	1.50	400	1.09	92.47 ± 3.72	7.22 ± 2.96
A4	2.00	403	1.63	88.53 ± 3.78	8.29 ± 3.18
A5	5.00	408	2.35	83.50 ± 5.94	9.84 ± 2.51

Notes: [a]Experiments were repeated three times and averaged; [b]Data were obtained by multiplying absorbance of the corresponding diluted solutions by their dilution factors when diluted solutions were used for the data; [c]Size of silver nanoparticles was determined by measuring diameters of about 100 nanoparticles in transmission electron microscopic image and by averaging them.

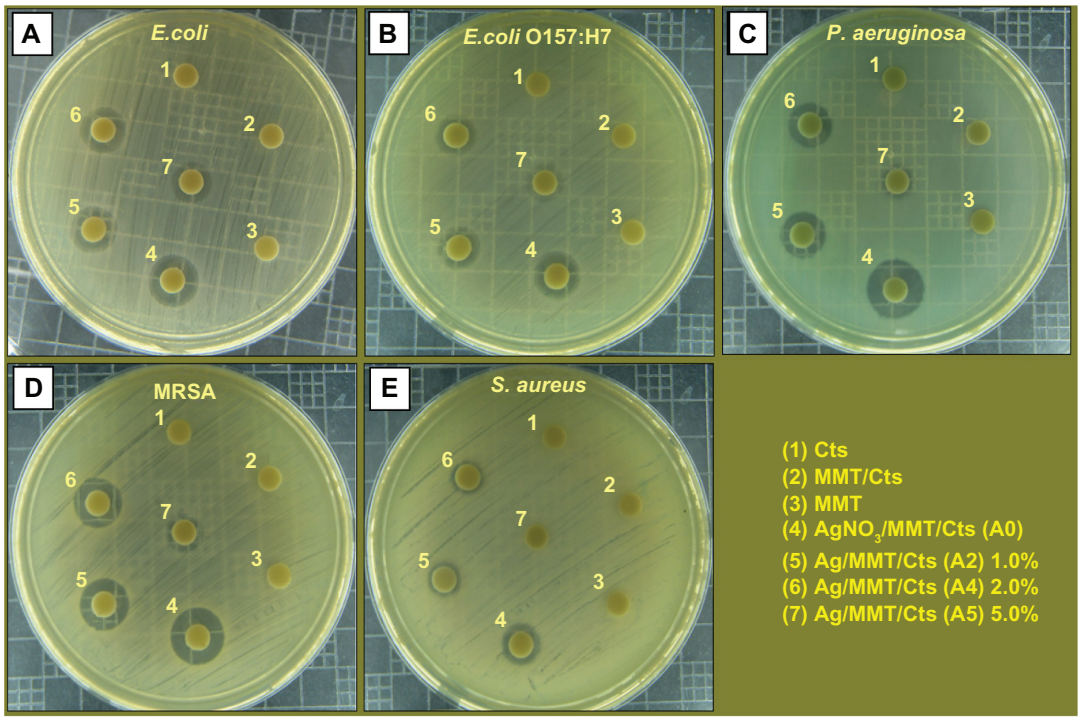

Figure 11 Comparison of the inhibition zone test between Gram-negative and Gram-positive bacteria, ie, *Escherichia coli* (**A**), *E. coli* O157:H7 (**B**), *Pseudomonas aeruginosa* (**C**), *Staphylococcus aureus* (**D**), and methicillin-resistant *S. aureus* (**E**).
Abbreviations: Cts, chitosan; MMT, montmorillonite.

P. aeruginosa, *S. aureus*, and MRSA. The results and images of the inhibition zones are presented as average values in Table 2 and Figure 11, respectively. Table 2 shows that the $AgNO_3$ and AgNPs in MMT/Cts suspension had high and similar antibacterial activity against Gram-negative and Gram-positive bacteria. Because of their size, AgNPs can easily reach the nuclear content of bacteria and they show a large and impressive surface area, where contact with bacteria is the greatest.[74,75] This could be the reason why these nanoparticles have the best antibacterial effect. For solid support systems, some researchers argue that Ag^+ ions released from the surface of AgNPs are responsible for their antibacterial activity.[76,77] For aqueous phase systems, the results show that the antibacterial test of Ag^+ ions is not high at the concentration levels reached by release, and the presence of AgNPs is very important, which reinforces the idea that the larger the surface area, the greater the antibacterial activity.[78] The diameters of the inhibition zones in agar plates are given in mm. The tests were repeated three times for each treated sample, and the results are presented in Table 2. The suspensions of MMT (10 mg/mL), soluble Cts (0.5 mg/mL), and MMT/Cts did not show any antibacterial activity. The $AgNO_3$/MMT/

Table 2 Average inhibition zone and standard deviation for montmorillonite, chitosan, montmorillonite/chitosan, silver/montmorillonite/chitosan bionanocomposites (A0), and silver/montmorillonite/chitosan bionanocomposites at different $AgNO_3$ concentrations: (A2) 1.0%, (A4) 2.0%, and (A5) 5.0%

Bacteria	Inhibition zone (mm)				Control negative (mm)			Control positive (mm)	
	A0	A2	A4	A5	MMT (10 mg/mL)	Cts (0.5 mg/mL)	MMT/ Cts (10:0.5 mg/mL)	CTX	C
E. coli	11.9	11.1	10.9	9.7	NA*	NA*	NA*	21.8	16.7
E. coli O157:H7	11.8	10.5	9.6	9.2	NA	NA	NA	20.4	18.3
P. aeruginosa	13.9	11.3	10.5	7.4	NA	NA	NA	19.3	17.6
S. aureus	9.8	8.4	7.8	6.8	NA	NA	NA	23.6	16.4
MRSA	13.2	11.9	11.40	9.3	NA	NA	NA	18.9	15.5

Notes: Mean standard deviation values for the *E. coli* ± 0.93 mm, *E. coli* O157:H7 ± 1.14 mm, *P. aeruginosa* ± 2.69 mm, *S. aureus* ± 1.25 mm, and MRSA ± 1.62 mm for A0, A2, A4, and A5.
Abbreviations: *NA, not appearing; MMT, montmorillonite; Cts, chitosan; *E. coli*, *Escherichia coli*; *E. coli* O157:H7, *Escherichia coli* O157:H7; *P. aeruginosa*, *Pseudomonas aeruginosa*; *S. aureus*, *Staphylococcus aureus*; MRSA, methicillin-resistant *Staphylococcus aureus*; CTX, cefotaxime; C, chloramphenicol.

Cts suspension for all tested bacteria shows high antibacterial activity and, interestingly, these effects in the Ag/MMT/Cts BNCs (A2, A4, and A5) were increased with decreasing size of AgNPs. However, this research also showed that the amounts of AgNPs gradually were increased in the Ag/MMT/Cts BNCs (A2, A4, and A5), but higher AgNPs loading does not lead to superior antibacterial activity.

Conclusion

AgNPs were successfully prepared from $AgNO_3$/MMT/Cts suspension at different $AgNO_3$ concentrations by using $NaBH_4$ as a chemical reduction agent in the interlamellar space and external layer surface of MMT modified with Cts without any heat treatment or reducing agent. These AgNPs were found to be stabilized by the low molecular weight of Cts. In addition, the distribution size of AgNPs prepared at different concentrations of $AgNO_3$ indicate that larger particle sizes of AgNPs were obtained when the Ag^+ ion concentration increased. The average diameters of the AgNPs were around 6.28, 8.29, and 9.84 nm for A2, A4, and A5, respectively. Moreover, the PXRD analysis confirmed that the crystallographic planes of the silver crystals were of the face-centered cubic type. The UV-visible absorption spectra showed the peak characteristics of the surface plasmon resonance bond of AgNPs. SEM images show that the external morphology for MMT, MMT/Cts and Ag/MMT/Cts BNCs (A2, A4, and A5) have layered surfaces with large flakes, with no noteworthy morphological distinctions between them. Also, due to the presence of AgNPs in the external and internal surfaces of Ag/MMT/Cts BNCs, these layers become shiny. EDXRF spectra confirmed the presence of elemental compounds in the MMT, Cts, and AgNPs without any contamination peaks. The antibacterial activities of Ag/MMT/Cts BNCs at the different AgNP particle sizes showed strong antibacterial activity against Gram-positive and Gram-negative bacteria. These results show that the antibacterial resistance of AgNPs in MMT/Cts can be modified according to the size of AgNPs, and decreases with increased particle size. Further studies are required to investigate the bactericidal effects of Ag/MMT/Cts BNCs against different types of bacteria for potential widening of their applications, such as in surgical devices and in drug-delivery vehicles.

Acknowledgments

The authors are grateful to the staff of the Department of Chemistry, Universiti Putra Malaysia, for their help with this research, and to the Institute of Bioscience, Universiti Putra Malaysia, for technical assistance.

Disclosure

The authors have no conflicts of interest to disclose in this work.

References

1. Carotenuto G, Pepe GP, Nicolais L. Preparation and characterization of nano-sized Ag/PVP composites for optical applications. *Eur Phys J B*. 2000;16:11–17.
2. Stathatos E, Lianos P. Photocatalytically deposited silver nanoparticles on mesoporous TiO_2 films. *Langmuir*. 2000;16:2398–2400.
3. Kyriacou SV, Brownlow WJ, Xu XN. Using nanoparticle optics assay for direct observation of the function of antimicrobial agents in single live bacterial cells. *Biochemistry*. 2004;43:140–147.
4. Feng X, Ma H, Huang S, et al. Aqueous-organic phase-transfer of highly stable gold, silver, and platinum nanoparticles and new route for fabrication of gold nanofilms at the oil/water interface and on solid supports. *J Phys Chem B*. 2006:110:12311–12317.
5. Choi S, Kim KS, Yeon SH, et al. Fabrication of silver nanoparticles via self-regulated reduction by 1-(2-hydroxyethyl)-3-methylimidazolium tetrafluoroborate. *Korean J Chem Eng*. 2007;24:856–859.
6. Kawashita M, Tsuneyama S, Mijaji F, et al. Antibacterial silver-containing silica glass prepared by the sol-gel method. *Biomaterials*. 2000;21:393–398.
7. Gauger A, Mempel M, Schekatz A, et al. Silver-coated textiles reduce *Staphylococcus aureus* colonization in patients with atopic eczema. *Dermatology*. 2003;207:15–21.
8. Lee HJ, Jeong SH. Bacteriostasis and skin innoxiousness of nanosize silver colloids on textile fabrics. *Text Res J*. 2005;75:551–556.
9. Ohashi S, Saku S, Yamamoto KJ. Antibacterial activity of silver inorganic agent YDA filler. *Oral Rehabil*. 2004;31:364–367.
10. Rupp ME, Fitzgerald T, Marion N, et al. Effect of silver-coated urinary catheters: Efficacy, cost-effectiveness, and antimicrobial resistance. *Am J Infect Control*. 2004;32:445–450.
11. Samuel U, Guggenbichler JP. Prevention of catheter-related infections: The potential of a new nano-silver impregnated catheter. *Int J Antimicrob Agents*. 2004;23:75–78.
12. Strathmann M, Wingender J. Use of an oxonol dye in combination with confocal laser scanning microscopy to monitor damage to *Staphylococcus aureus* cells during colonisation of silver-coated vascular grafts. *Int J Antimicrob Agents*. 2004;24:234–240.
13. Bosetti M, Masse A, Tobin E, et al. Silver coated materials for external fixation devices: In vitro biocompatibility and genotoxicity. *Biomaterials*. 2002;23:887–892.
14. Alt V, Bechert T, Steinrücke P, et al. An in vitro assessment of the antibacterial properties and cytotoxicity of nanoparticulate silver bone cement. *Biomaterials*. 2004;25:4383–4391.
15. Ulkur E, Oncul O, Karagoz H, et al. Comparison of silver-coated dressing (Acticoat™), chlorhexidine acetate 0.5% (Bactigrass®), and fusidic acid 2% (Fucidin®) for topical antibacterial effect in methicillin-resistant staphylococci-contaminated, full-skin thickness rat burn wounds. *Burns*. 2005;31:874–877.
16. Parikh DV, Fink T, Rajasekharan K, et al. Antimicrobial silver/sodium carboxymethyl cotton dressings for burn wounds. *Text Res J*. 2005;75:134–138.
17. Gosheger G, Hardes J, Ahrens H, et al. Silver-coated megaendoprostheses in a rabbit model an analysis of the infection rate and toxicological side effects. *Biomaterials*. 2004;25:5547–5556.
18. Chou WL, Yu DG, Yang MC. The preparation and characterization of silver-loading cellulose acetate hollow fiber membrane for water treatment. *Polym Adv Technol*. 2005;16:600–607.
19. Yuranova T, Rincon AG, Bozzi A, et al. Antibacterial textiles prepared by RF-plasma and vacuum-UV mediated deposition of silver. *Photochem Photobiol A*. 2003;161:27–34.

20. Jeong SH, Yeo SY, Yi SC. The effect of filler particle size on the antibacterial properties of compounded polymer/silver fibers. *J Mater Sci*. 2005;40:5407–5411.
21. Sun RWY, Chen R, Chung NPY, et al. Silver nanoparticles fabricated in Hepes buffer exhibit cytoprotective activities toward HIV-1 infected cells. *Chem Commun*. 2005;40:5059–5061.
22. Matijevic E. Preparation and properties of uniform size colloids. *Chem Mater*. 1993;5:412–426.
23. Nickel U, Castell AZ, Poppl K, et al. A silver colloid produced by reduction with hydrazine as support for highly sensitive surface-enhanced raman spectroscopy. *Langmuir*. 2000;16:9087–9091.
24. Leopold N, Lendl BJ. A new method for fast preparation of highly surface-enhanced raman scattering (SERS) active silver colloids at room temperature by reduction of silver nitrate with hydroxylamine hydrochloride. *Phys Chem B*. 2003;107:5723–5727.
25. Khanna PK, Subbarao VVVS. Nanosized silver powder via reduction of silver nitrate by sodium formaldehydesulfoxylate in acidic pH medium. *Mater Lett*. 2003;57:2242–2245.
26. Sondi I, Goia DV, Matijevic EJJ. Preparation of highly concentrated stable dispersions of uniform silver nanoparticles. *Colloid Interface Sci*. 2003;260:75–81.
27. Morones JR, Elechiguerra JL, Camacho A, et al. The bactericidal effect of silver nanoparticles. *Nanotechnology*. 2005;16:2346–2353.
28. Baker C, Pradhan A, Pakstis L, et al. Synthesis and antibacterial properties of silver nanoparticles. *Nanosci Nanotechnol*. 2005;5:244–249.
29. Yong KT, Sahoo Y, Swihart MT, et al. Synthesis and plasmonic properties of silver and gold nanoshells on polystyrene cores of different size and of gold–silver core–shell nanostructures. *Colloids and Surfaces A*. 2006;290:89–105.
30. Shameli K, Ahmad MB, Yunus WMZW, et al. Silver/poly(lactic acid) nanocomposites: Preparation, characterization, and antibacterial activity. *Int J Nanomedicine*. 2010;5:573–579.
31. Shen J, Shi M, Li N, et al. Facile synthesis and application of Ag-chemically converted graphene nanocomposites. *Nano Res*. 2010;3:339–349.
32. Wu ML, Chen DH, Huang TC. Evidence for seed-mediated nucleation in the chemical reduction of gold salts to gold nanoparticles. *Chem Mater*. 2001;13:2313–2322.
33. Underhill RS, Liu G. Preparation and performance of Pd particles encapsulated in block copolymer nanospheres as a hydrogenation catalyst. *Chem Mater*. 2000;12:3633–3641.
34. Torigoe K, Suzuki A, Esumi K. Au (III)–PAMAM interaction and formation of Au–PAMAM nanocomposites in ethyl acetate. *J Colloid Interface Sci*. 2001;241:346–356.
35. Henglein A, Giersig M. Reduction of Pt (II) by H_2: Effects of citrate and NaOH and reaction mechanism. *J Phys Chem B*. 2000;104:6767–6772.
36. Mayer ABR, Grebner W, Wannemacher R. Preparation of silver-latex composites. *J Phys Chem B*. 2000;104:7278–7285.
37. Han MY, Quek CH, Huang W, et al. A simple and effective chemical route for the preparation of uniform nonaqueous gold colloids. *Chem Mater*. 1999;11:1144–1147.
38. Yin Y, Li Z-Y, Zhong Z, et al. Synthesis and characterization of stable aqueous dispersions of silver nanoparticles through the Tollens process. *J Mater Chem*. 2002;12:522–527.
39. Wang Y, Ren J, Deng K, et al. Preparation of tractable platinum, rhodium, and ruthenium nanoclusters with small particle size in organic media. *Chem Mater*. 2000;12:1622–1627.
40. Pathak S, Greci MT, Kwong RC, et al. Synthesis and applications of palladium-coated poly(vinylpyridine) nanospheres. *Chem Mater*. 2000;12:1985–1989.
41. Tan Y, Li Y, Zhu D. Preparation of silver nanocrystals in the presence of aniline. *J Colloid Interface Sci*. 2003;258:244–251.
42. Wang J, Neoh KG, Kang ET. Preparation of nanosized metallic particles in polyaniline. *J Colloid Interface Sci*. 2001;239:78–86.
43. Lim B, Jiang M, Yu T, et al. Nucleation and growth mechanisms for Pd–Pt bimetallic nanodendrites and their electrocatalytic properties. *Nano Res*. 2010;3:69–80.
44. Changa JH, Ana YU, Cho D, et al. Poly (lactic acid) nanocomposites: Comparison of their properties with montmorillonite and synthetic mica (II). *Polymer*. 2003;44:3715–3720.
45. Chang JH, An YU, Sur GS. Poly (lactic acid) nanocomposites with various organoclays. I. Thermomechanical properties, morphology, and gas permeability. *J Polym Sci B Pol Phys*. 2003;41:94–103.
46. Giannelis EP, Krishnamoorti R, Manias E. Polymer-silicate nanocomposites: Model systems for confined polymers and polymer brushes. *Adv Polym Sci*. 1999;138:107–147.
47. Ramsay JDF, Swanton SW, Bunce JJ. Swelling and dispersion of smectite caly colloids: Determination of structure by neutron diffraction and small-angle neutron scattering. *J Chem Soc Faraday Trans*. 1999;86:3919–3926.
48. Ahmad MB, Shameli K, Darroudi M, et al. Synthesis and characterization of silver/clay nanocomposites by chemical reduction method. *Am J Appl Sci*. 2009;6:1909–1914.
49. Gao Y, Yunzhao Y. Deposition of silver nanoparticles on montmorillonite platelets by chemical plating. *J Mater Sci*. 2002;37:5083–5087.
50. Wang S-F, Shen L, Zhang W-D, et al. Preparation and mechanical properties chitosan/carbon nanotubes composites. *Biomacromolecules.* 2005;6:3067–3072.
51. Darder M, Colilla M, Ruiz-Hitzky E. Chitosan-clay nanocomposites: Application as electrochemical sensors. *Appl Clay Sci*. 2005;28:199–208.
52. Zhou NL, Liu Y, Li L, et al. A new nanocomposite biomedical material of polymer/clay-Cts-Ag nanocomposites. *Curr Appl Phys*. 2007;7S1:58–62.
53. Ahmad MB, Shameli K, Darroudi M, et al. Synthesis and antibacterial activity of silver/montmorillonite nanocomposites. *Res J Biol Sci.* 2009;4:1032–1036.
54. O'Hanlon SJ, Enright MC. A novel bactericidal fabric coating with potent in vitro activity against methicillin-resistant Staphylococcus aureus (MRSA). *Int J Antimicrob Agents*. 2009;33:427–431.
55. Holtz RD, Filho AGS, Brocchi M, Martins D, Durán N, Alves OL. Development of nanostructured silver vanadates decorated with silver nanoparticles as a novel antibacterial agent. *Nanotechnology*. 2010;21:1–8.
56. Lara HH, Ayala-Nuñez NV, Ixtepan-Turrent L, Rodriguez-Padilla C. Mode of antiviral action of silver nanoparticles against HIV-1. *J Nanobiotechnology*. 2010;8:1–10.
57. Medina-Ramirez I, Bashirb S, Luo Z, et al. Green synthesis and characterization of polymer-stabilized silver nanoparticles. *Colloids Surf B Biointerfaces.* 2009;73:185–191.
58. Shameli K, Ahmad MB, Yunus WMZW, et al. Synthesis and characterization of silver/talc nanocomposites using the wet chemical reduction method. *Int J Nanomedicine*. 2010;5:743–751.
59. Darroudi M, Ahmad MB, Shameli K, et al. Synthesis and characterization of UV-irradiated silver/montmorillonite nanocomposites. *Solid State Sci*. 2009;11:1621–1624.
60. Ahmad MB, Shameli K, Yunus WMZW, et al. Synthesis and characterization of silver/clay/starch bionanocomposites by green method. *Aust J Basic Appl Sci*. 2010;4:2158–2165.
61. Shameli K, Ahmad MB, Yunus WMZW, et al. Green synthesis of silver/montmorillonite/chitosan bionanocomposites using the UV irradiation method and evaluation of antibacterial activity. *Int J Nanomedicine*. 2010;5:875–887.
62. Ahmad MB, Shameli K, Darroudi M, et al. Synthesis and characterization of silver/clay/chitosan bionanocomposites by UV-irradiation method. *Am J Appl Sci*. 2009;6:2030–2035.
63. Song KC, Lee MS, Park TS, et al. Preparation of colloidal silver nanoparticles by chemical reduction method. *Korean J Chem Eng*. 2009;26:153–155.
64. Aihara N, Torigoe K, Esumi K. Preparation and characterization of gold and silver nanoparticles in layered laponite suspensions. *Langmuir*. 1998;14:4945–4949.

65. Xu G-N, Qiao X-L, Qiu X-L, et al. Preparation and characterization of stable monodisperse silver nanoparticles via photoreduction. *Colloids and Surfaces A*. 2008;320:222–226.
66. Liu Z, Wang H, Wang LX. Red shift of plasmon resonance frequency due to the interacting Ag nanoparticle embedded in single crystal SiO_2 by implantation. *Appl Phys Lett.* 1998;72:1823–1825.
67. Patakfalvi RA, Oszka A, Dekany I. Synthesis and characterization of silver nanoparticles/kaolinite composites. *Colloids Surf A Physicochem Eng Asp*. 2003;220:45–54.
68. Shin HS, Yang HJ, Kim SB, et al. Mechanism of growth of colloidal silver nanoparticles stabilized by polyvinyl pyrrolidone in γ-irradiated silver nitrate solution. *J Colloid Interface Sci*. 2004;274:89–94.
69. Bar H, Bhui DK, Sahoo GP, et al. Green synthesis of silver nanoparticles using latex of *Jatropha curcas*. *Colloids and Surf A*. 2009;339:134–139.
70. Alemdar A, Güngör N, Ece OI, et al. The rheological properties and characterization of bentonite dispersions in the presence of non-ionic polymer PEG. *J Mater Sci*. 2005;40:171–177.
71. Günister E, Pestreli D, Ünlü CH, et al. Synthesis and characterization of chitosan-MMT biocomposite systems. *Carbohyd Polym*. 2007;67:358–365.
72. Darder M, Colilla M, Ruiz-Hitzky E. Biopolymer-clay nanocomposites based on chitosan intercalated in montmorillonite. *Chem Mater.* 2003;15:3774–3780.
73. Benn TM, Westerhoff P. Nanoparticle silver released into water from commercially available sock fabrics. *Environ Sci Technol*. 2008;42:4133–4139.
74. Chudasama B, Vala AV, Andhariya N, et al. Enhanced antibacterial activity of bifunctional Fe_3O_4 core-shell nanostructures. *Nano Res*. 2009;2:955–965.
75. Chen SF, Li JP, Qian K, et al. Large scale photochemical synthesis of M2TiO2 nanocomposites (M = Ag, Pd, Au, Pt) and their optical properties, CO oxidation performance, and antibacterial effect. *Nano Res*. 2010;3:244–255.
76. Morones JR, Elechiguerra JL, Camacho A, et al. The bactericidal effect of silver nanoparticles. *Nanotechnology*. 2005;16:2346–2353.
77. Lee D, Cohen RE, Rubner MF. Antibacterial properties of Ag nanoparticle loaded multilayers and formation of magnetically directed antibacterial microparticles. *Langmuir*. 2005;21:9651–9659.
78. Jeong SH, Hwnag YH, Yi SC. Antibacterial properties of padded PP/PE nonwovens incorporating nano-sized silver colloids. *J Mater Sci*. 2005;40:5413–5418.